Chemical characterization and source apportionment of fine particulate matter in Eastern Africa using aerosol mass spectrometry.

Supporting Information:

Theobard Habineza[1], Allen L. Robinson[2], H. Langley DeWitt[3], Jimmy Gasore[4], Philip L. Croteau[5], Albert A. Presto[*1,4]

[1]Carnegie Mellon University, Department of Mechanical Engineering and Center for Atmospheric Particle Studies (CAPS)

[2]Department of Atmospheric Science, Colorado State University

[3]CIRES, University of Colorado, Boulder, CO, USA

[4] Kigali Collaborative Research Center, Kigali, Rwanda

[5]Aerodyne Research, Inc., Billerica, Massachusetts, USA

*_Corresponding to_: apresto@andrew.cmu.edu

I. Sampling location

Figure S1: Sampling location

The sampling location is situated at latitude -1.9619 and longitude 30.0645, at an altitude of about 1500 meters above sea level within Kigali City, Nyarugenge District, Rwanda. This site lies within the Intertropical Convergence Zone (ITCZ), where the sun rises around 6:00 AM and sets around 6:00 PM throughout the year. The weather conditions at this site are moderate across all seasons, with an annual average temperature ranging from 17°C to 24°C countrywide(Meteo Rwanda, 2025).

The rainfall pattern in this region is characterized by four alternating seasons: Two dry seasons: June–August (JJA) and December–February (DJF). Two rainy seasons: March-May (MAM) and September–

November (SON). The annual mean precipitation at this site ranges between 1,100 mm and 1,300 mm, as it is in the central part of the country(World Bank, 2025).

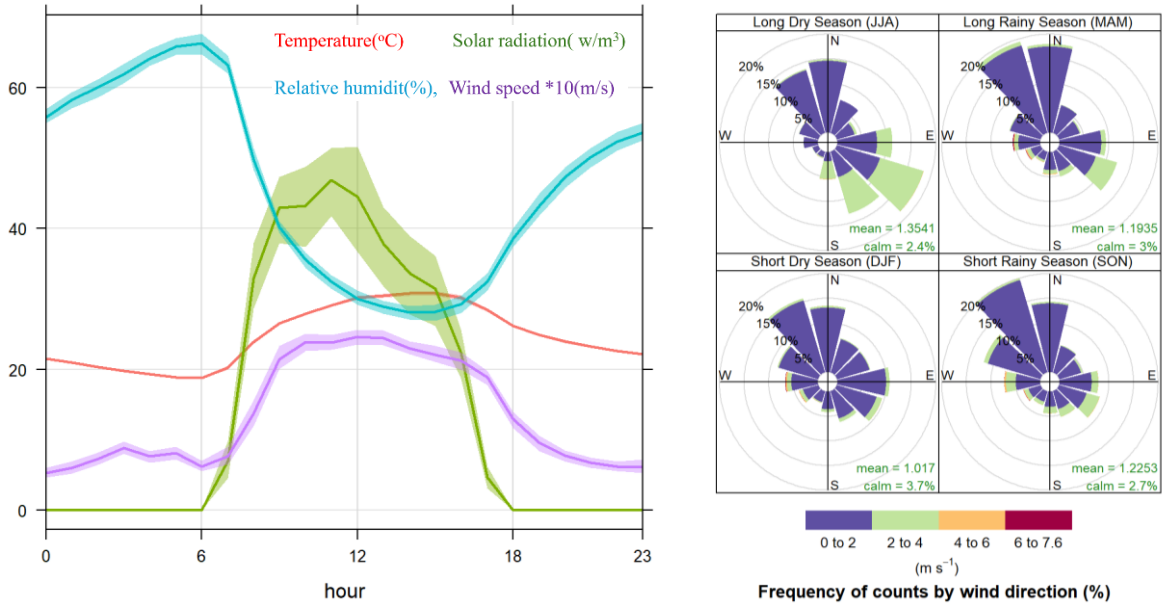

Figure S2: Diurnal variations of meteorological parameters recorded at Kivugiza station, approximately 5 km from the monitoring site. (a) Shows hourly averages of temperature (°C), solar radiation (W/m²), relative humidity (%), and 10x wind speed (m/s). Shaded regions represent standard deviations from the mean. (b) Displays seasonal wind rose plots for JJA (June–August), MAM (March), DJF (December–February), and SON (September–November), illustrating prevailing wind directions and intensities.

A wind rose and diurnal plot diagram for the wind measured 2 meters in height along with the direction frequency across four seasons obtained at Kivugiza meteorological station from May 2023 to May 2024 shows that winds predominantly come from the north and northwest. Wind speeds mostly range between 0–4 m/s, with the strongest winds occurring during the Long Dry Season (JJA, mean = 1.35 m/s) and the weakest in the Short Dry Season (DJF, mean = 1.02 m/s, calm = 3.7%). The long rainy season (MAM, mean = 1.19 m/s) and short rainy season (SON, mean = 1.22 m/s) show moderate wind activity. Higher wind speeds above 4 m/s are rare. Overall, winds remain moderate throughout the year.

PM_1 vs $PM_{2.5}$ and seasonal variability in PM_1 components

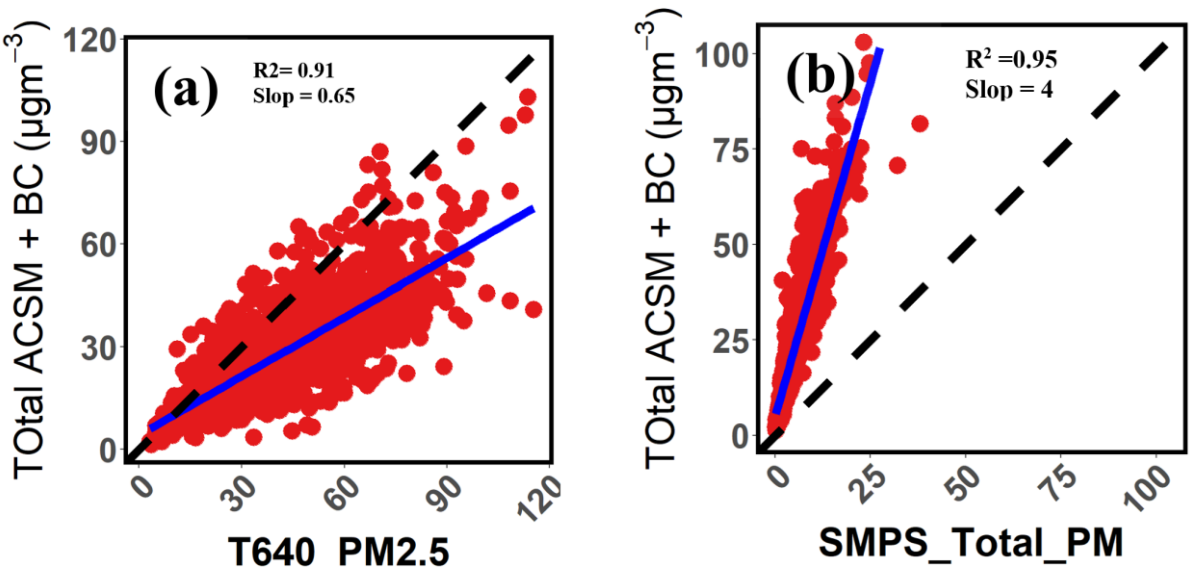

Figure S3: (a) Comparison of PM_1 (NR_PM1+BC) with $PM_{2.5}$ measured at the US Embassy. (b) NR_PM_1+BC versus SMPS (scanning mobility particle sizer).

The annual mean PM_1 (particles with an aerodynamic diameter of less than 1 µm) in Kigali constitutes 65% of $PM_{2.5}$. Organic components dominate in all seasons, with their proportion peaking during the long dry season (75% of total PM_1) and being slightly lower during the short rainy season (73% of total PM_1). Black Carbon (BC) is the second-largest component, with its contribution ranging between 15% and 22%. The highest BC composition was observed during the long rainy season, showing a similar trend to Abidjan, Côte d'Ivoire(Anand et al., 2024).

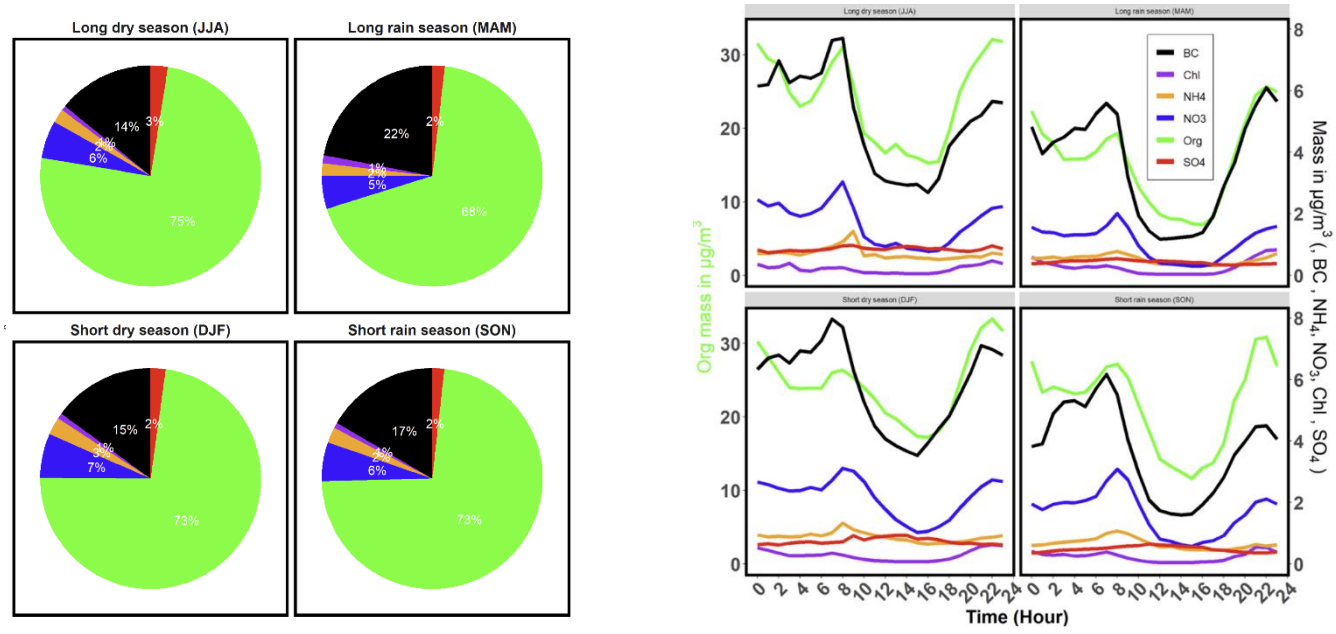

Figure S4: (Left) Seasonal averages of PM1 composition. (Right) Diurnal variation of PM1 component concentrations by seasons. For all the panels the left y-axis represents the organic component's concentrations whereas the right y-axis represents the concentration of inorganic (NH4, NO3, SO4, and Chl) species and BC.

The diurnal patterns during the dry seasons show a higher magnitude on an hourly basis compared to those in the rainy season. However, SO_4 remained relatively constant across all four seasons. The JJA season exhibits the highest morning and evening peaks, reflecting the influence of morning rush hour emissions, a shallower planetary boundary layer height, and the absence of major PM removal processes such as precipitation scavenging.

II. Particle organic nitrate vs inorganic nitrate.

Particle nitrate can be quantified using different approaches in literature(Werden et al., 2023) used Equation 1 to quantify the fraction of particle organic nitrate.

$$p_{OrgNo3\left(\frac{\mu g}{m^3}\right)} = NO_3 * \frac{(R_{ambient} - R_{pNO3}) * (1 + 0.1)}{(0.1 - R_{pNH_4NO_3}) * (1 + R_{ambient})} \quad (1)$$

Day et al. (Day et al., 2022) used equation two to quantify the particle organic nitrate.

$$f_{pOrgNo3} = \frac{(R_{ambient} - R_{pNO3}) * (1 + R_{porgNO3})}{(R_{porgNO3} - R_{pNH_4NO_3}) * (1 + R_{ambient})} \quad (2)$$

with $R_{pOrgNO3}$ inferred as R_{pNO3}/RoR**,** Day, et al. suggest that in the absence of direct measurements of the RoR, the standard value could be 2.75 ± 0.75**.**

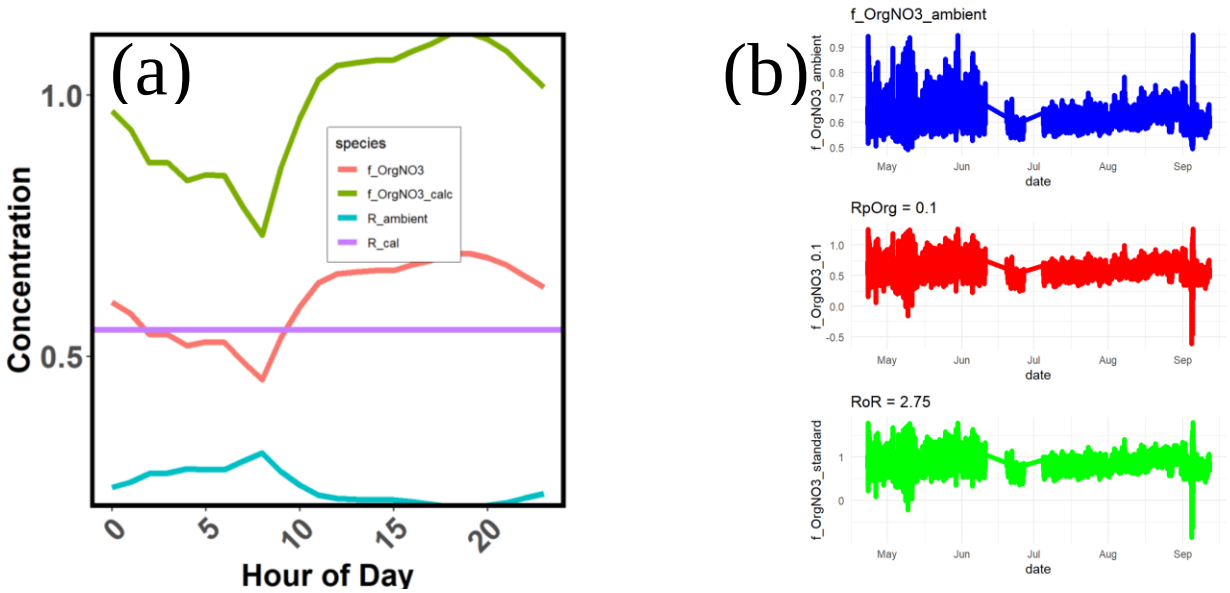

Figure S5: (a), Diurnal patterns of the fraction of organic nitrate, shown in green and red, alongside the ratio of m/z 30 to m/z 46 from NH_4NO_3 calibration (purple) and ambient measurements (blue). (b),Particle-phase organic nitrate fraction was estimated using a standard ROR value of 2.75, assuming RpOrg = 0.1 and the ambient measurement-derived organic nitrate fraction.

Figure S5 (a) presents the diurnal variation of the fractional contribution of organic nitrate using standard ROR and ambient measurement delivered ROR approaches, while panel (b) shows the time series contribution of particle organic nitrate at the site for the three methods. At this site, we examined both

quantification approaches, and Figure S5 illustrates the results. The calculated NO_2/NO ratios for ambient and calibration conditions were $R_{NH4NO3\ calibration} = 0.56 \pm 0.83$. Using ambient observations ($R_{ambient} = 0.25 \pm 0.06$) and a representative organonitrate ratio ($RoR = 2.5 \pm 1.05$), we estimated the average particle-phase organic nitrate fraction to be 61% ± 17%. Applying the approach by Werden et al. (assuming pOrgNitrate = 0.1) yielded a comparable result of 61% ± 14.6%, with minimal diurnal variability—62% during the day and 63% at night. In contrast, using the method from Day et al. ($RoR = 2.7 \pm 0.75$) resulted in an organic nitrate fraction of 98% ± 23.5%, which in some cases exceeded 100%, indicating overestimation. Given the consistency of the Werden-based estimate and the unrealistic output from Day et al.'s method, we adopted the direct calculation approach using the expression $pOrgNitrate = PNO_3 / RoR$. This supports the conclusion that, on average, 61% of the nitrate in Kigali is organic, while the remaining 39% is present as inorganic ammonium nitrate.

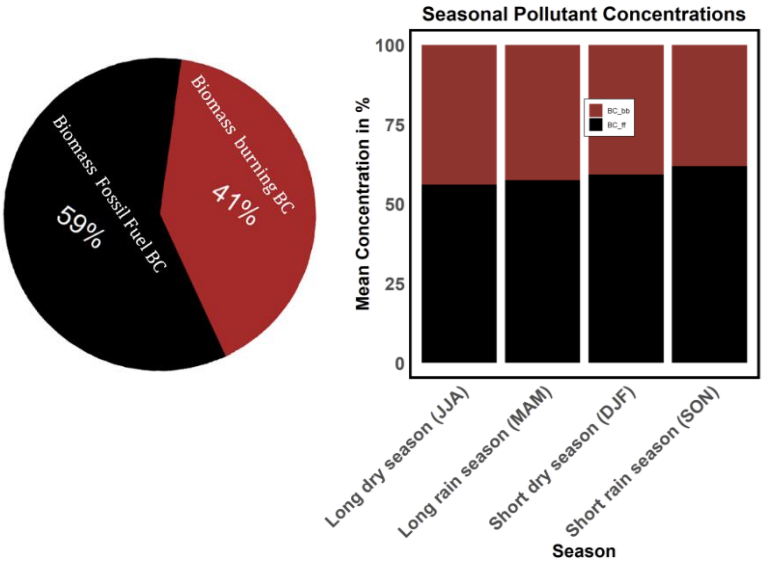

Figure S6: Overall (left) and seasonal (right) attribution of BC to fossil fuel and biomass burning sources.

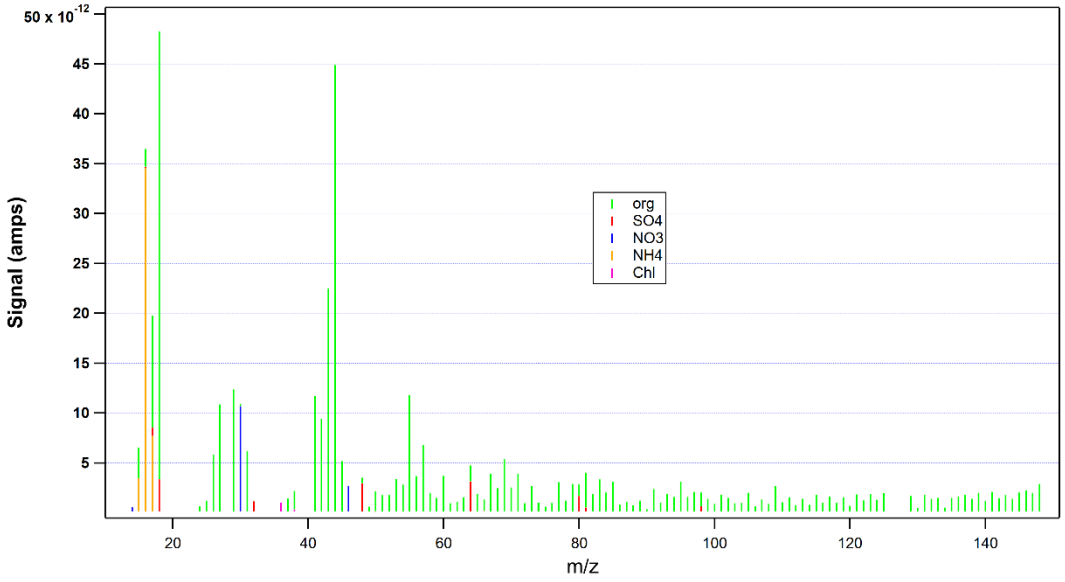

Figure S7: Average Mass spectra from the Q-ACSM

III. PMF output and diagnostic plots

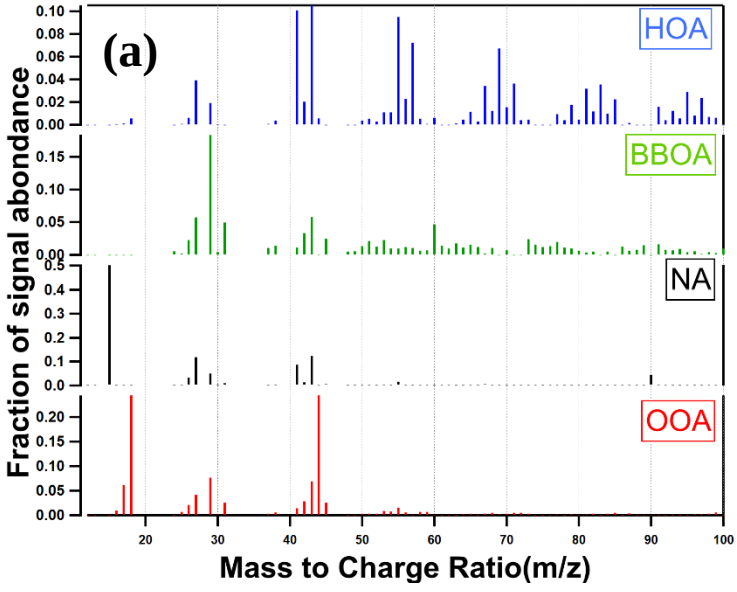

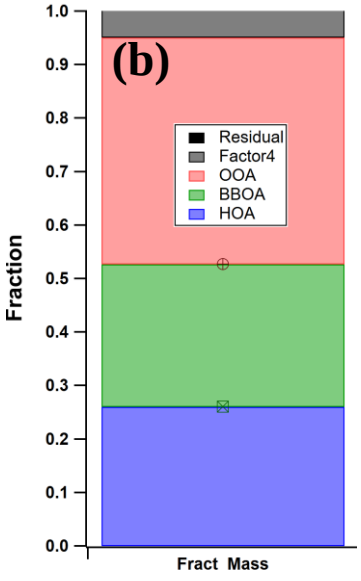

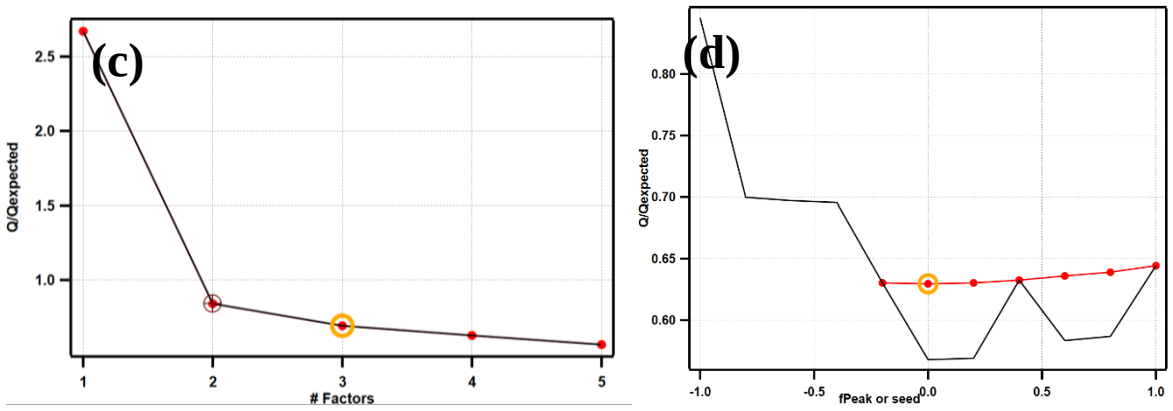

Figure S8: PMF output. Panel (a) shows the source profiles for a 4-factor solution and panel (b) shows the mass attributed to each factor. Panel (c) shows the Q/Qexp as a function of the number of factors, and (d) shows how Q/Qexp changes with peak for the three-factor solution.

Three-factor source profiles were selected as the most suitable PMF solutions with FPEAK = 0. The solution was chosen based on the individual source-normalized contribution to the overall mass loading, the total sum of the square of the scaled residuals (Q) to the expected ratio (Qexp), the comparison of source spectra to standard spectra, as well as the residual factor and the correlation between R_ time series and R_ spectra.

With a three-factor solution at FPEAK = 0, the Q/Qexp value was 0.6936, compared to 0.84349 for a two-factor PMF solution. In the four-factor solution, the Q/Qexp value further decreased to 0.62963, indicating no significant improvement in source separation at the station.

The two-factor solution resolved an OOA factor and a mixed HOA+BBOA factor. This solution was not selected because both biomass burning and vehicle emissions (HOA) are expected to be important sources in Kigali.

Figure S8 (a) and (b) show the results of a 4-factor PMF solution. It included factors for HOA, BBOA, OOA, and a fourth unknown factor. A source profile is considered significant if it contributes at least 10% of the total mass load(Paatero & Tapper, 1994; Reff et al., 2007) The fourth factor contributed only 6%, whereas OOA accounted for 42%, BBOA for 27%, HOA for 26%, and the remaining 1% was residual.

The fourth factor in the four-factor solution did not resemble any standard source profile and remained unstable across seasons.

IV. Comparison of PMF source profiles with the external measurement and tracer ions.

a)

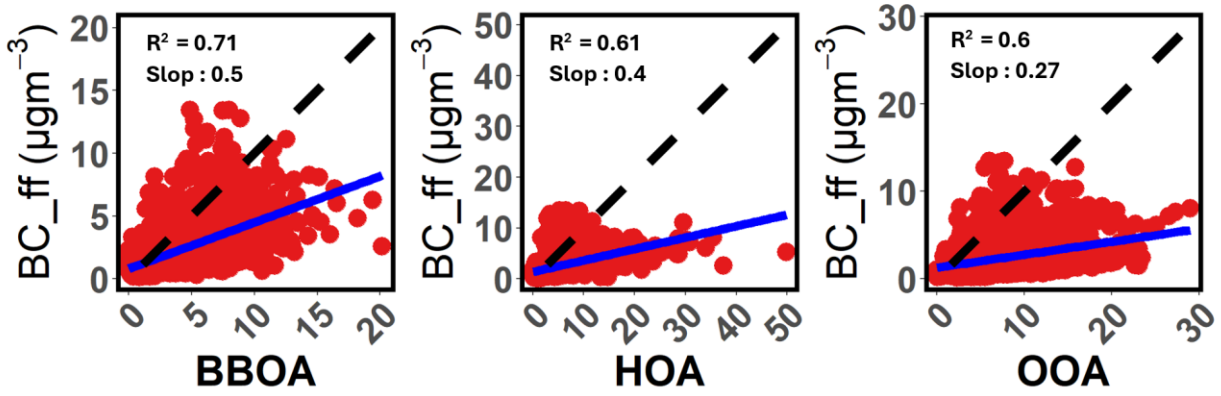

b)

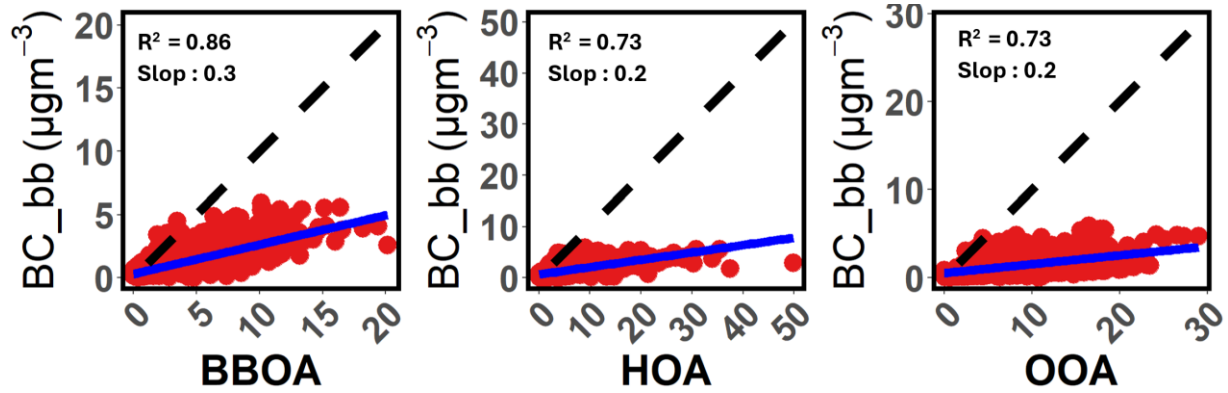

c)

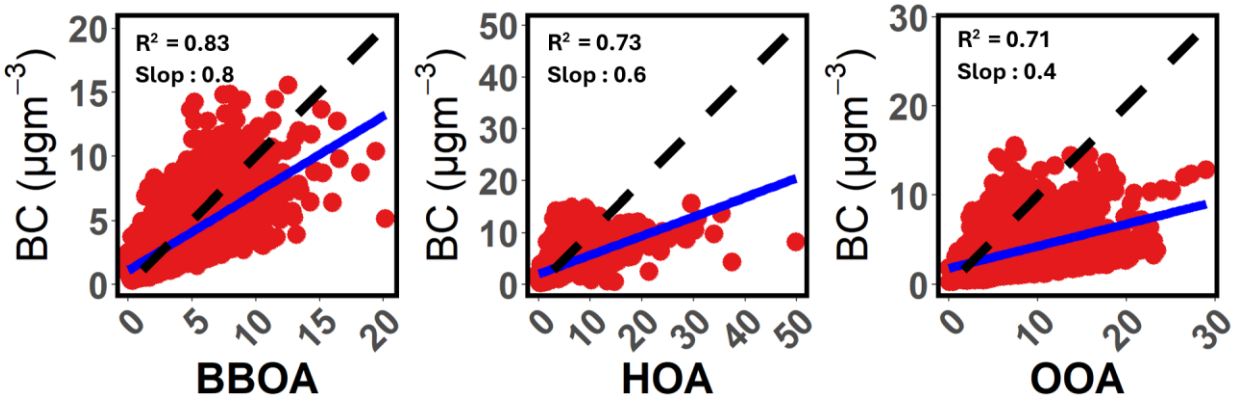

Figure S9: Comparison of the delivered source profiles and ambient measurements. ((a) source profiles with BC fraction from fossil fuel combustion, (b) source profile with the BC from Biomass burning fraction, (c) source profiles with the total black carbon)

Comparison of the source profiles' spectra and the reference spectra in the literature(Colorado state university, 2025).

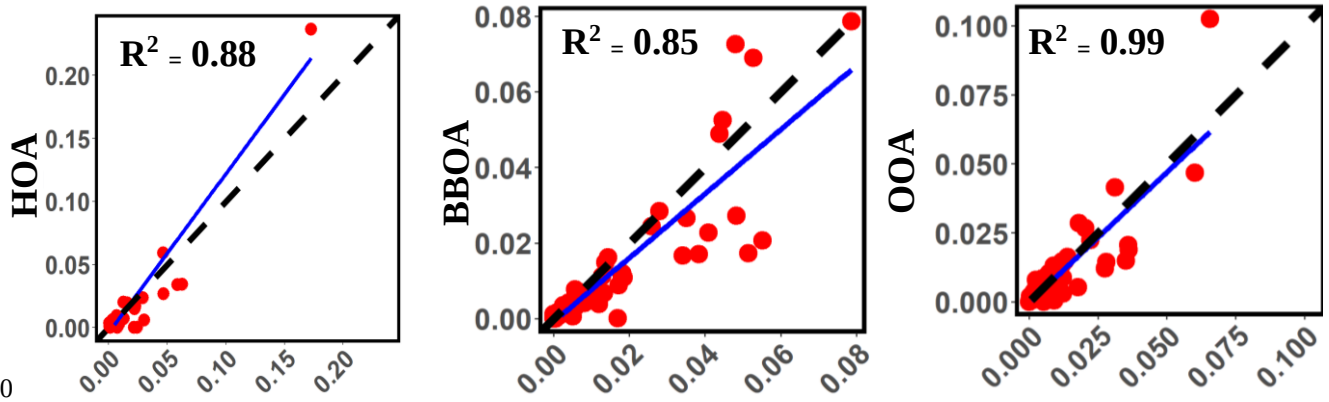

Figure S10: Source profiles spectra vs standard spectra

The source profile comparison includes:

a) BC from fossil fuel burning (BC_ff), b) BC from biomass burning (BC_bb), c) Total Black Carbon, and

d) Standard spectral profiles. All the delivered source profiles correlate with the reference mass spectra; however, OOA showed a good correlation, whereas HOA and BBOA exhibited a strong correlation with

the standard spectral profile, panel (c).

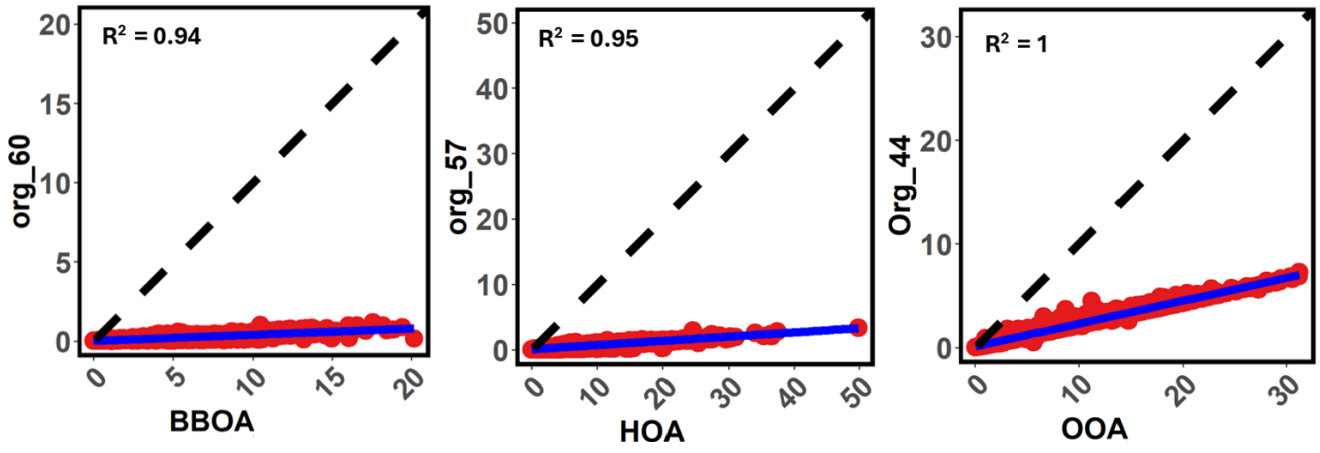

Figure S11: Source profiles vs the tracer ions

All the delivered source profiles correlate well with the individual average mass concentrations of the tracer ions (HOA vs. mz57, BBOA vs. mz60, and OOA vs. mz44)

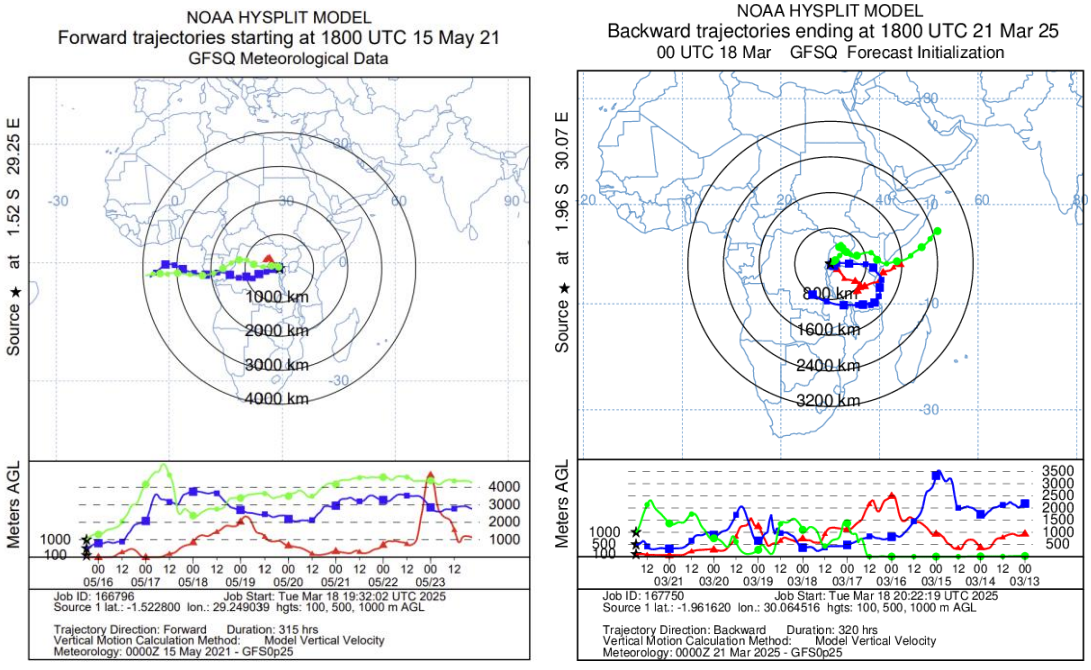

Figure S12: Forward trajectory at Nyiragogongo volcano and backward trajectory analysis of the air masses In Kigali during the Nyiragongo eruption.

The forward trajectory indicates that the emissions of Nyiragongo are transported in the west and no air emissions are transported to the Rwanda side and the back trajected analysis at the Kigali site indicates that the station receives easterly wind originating from Tanzania.

Reference

1. Meteo Rwanda. Climatology of eastern Africa. *https://www.meteorwanda.gov.rw/index.php?id=30&L=0* (2025).
2. World Bank. Rwanda Climatology. *climateknowledgeportal.worldbank.org/country/rwanda/climate-data-historical visited 2025_Feb_12 20:44 EST _* (2025).
3. Anand, A. *et al.* Low-Cost Hourly Ambient Black Carbon Measurements at Multiple Cities in Africa. *Environ Sci Technol* **58**, 12575–12584 (2024).
4. Werden, B. S. *et al.* Submicron Aerosol Composition and Source Contribution across the Kathmandu Valley, Nepal, in Winter. *ACS Earth Space Chem* **7**, 49–68 (2023).
5. Day, D. A. *et al.* A systematic re-evaluation of methods for quantification of bulk particle-phase organic nitrates using real-Time aerosol mass spectrometry. *Atmos Meas Tech* **15**, 459–483 (2022).
6. Reff, A., Eberly, S. I. & Bhave, P. V. Receptor modeling of ambient particulate matter data using positive matrix factorization: Review of existing methods. *J Air Waste Manage Assoc* **57**, 146–154 (2007).
7. Paatero, P. & Tapper, U. Positive matrix factorization: A non-negative factor model with optimal utilization of error estimates of data values. *Environmetrics* **5**, 111–126 (1994).
8. Colorado state university. AMS Spectral Database . *https://cires1.colorado.edu/jimenez-group/AMSsd/* (2025).